

## Elastic and Inelastic Scattering of $\alpha$ Particles and Protons from $^{144}\text{Sm}^\dagger$

J. H. Barker\* and J. C. Hiebert

Texas A&M University, College Station, Texas 77843

(Received 14 June 1971)

Differential cross sections for the elastic scattering and inelastic scattering to the low-lying states in  $^{144}\text{Sm}$  have been measured using 50-MeV  $\alpha$ -particle and 30-MeV proton beams from the Texas A&M variable-energy cyclotron. Spin and parity assignments are checked and transition strengths measured for states at 1.66, 1.81, and 2.19 MeV. A  $2^+$  assignment is made for a state at  $2.45 \pm 0.02$  MeV. The angular distributions are analyzed in the distorted-wave Born approximation, employing collective-model form factors. The present results are compared with previous experimental data and with recent theoretical calculations of the states in  $^{144}\text{Sm}$ .

### I. INTRODUCTION

The  $N=82$  isotones have recently been the subject of a large number of theoretical<sup>1-3</sup> and experimental<sup>4-7</sup> studies. These studies have been motivated to a large extent by the hope that the closed-shell nature of these nuclei will allow their low-lying excited states to be described by shell-model configurations involving only those protons outside the  $Z=50$  closed shell.

The nucleus  $^{144}\text{Sm}$  has been studied in some detail,<sup>7-13</sup> but many spectroscopic quantities remain to be determined. Only one  $B(E1)$  has been measured and some discrepancies still exist in the spin and parity assignments of some of the low-lying levels.

By performing two independent but related experiments we have attempted to eliminate some of the gaps in the knowledge of the structure of  $^{144}\text{Sm}$ . In particular, we suggest a solution to the problem of the spin and parity assignment of a level at 2.45–2.48-MeV excitation by proposing the existence of two distinct levels. We also present a comparison of these transition rates to other experimental<sup>13</sup> and theoretical<sup>3</sup> values using the methods suggested by Bernstein.<sup>14</sup>

### II. DESCRIPTION OF EXPERIMENTS

#### $\alpha$ Beam and Its Detection

A 49.4-MeV beam of  $\alpha$  particles was accelerated by the Texas A&M cyclotron and transported via a  $159.5^\circ$ ,  $n=\frac{1}{2}$  magnet, fitted with 2.54-mm entrance and exit slits, to a 60-cm-diam scattering chamber located at the end of beam line 7 (see Fig. 1). The analyzing magnet slits produce a beam energy resolution of approximately 50 keV full width at half maximum (FWHM). The exit slits and a final set of slits located just prior to the second switching magnet were made of 0.29-

mm tantalum in order to minimize slit-edge scattering. No slits were placed in the scattering chamber. All collimators were thus located such that slit-scattered  $\alpha$  particles would have to traverse at least two magnetic elements and would hopefully be removed from the beam. These steps taken to minimize slit-edge scattering contributions to the small-angle data allowed us to obtain quite clean spectra. For scattering angles less than  $18^\circ$ , where the contaminant elastic peaks were resolved from the 1.66-MeV inelastic peak, the background in the region of the latter peak was 4 orders of magnitude smaller than the elastic peak. A typical spectrum is shown in Fig. 2.

Both a monitor detector and a Faraday cup were used to establish relative normalization. Absolute cross sections were obtained by normalizing the elastic scattering data to Rutherford scattering at forward angles.

The determination of the energy of the beam as well as a determination of any zero-angle correction was accomplished with a crossover technique<sup>15</sup> using a polystyrene target. In some of the later work, the beam energy was determined using the calibration of the analyzing magnet.<sup>16</sup>

The scattered  $\alpha$  particles were detected in a pair of 1500- $\mu$  surface-barrier detectors. The signals from the detectors were sent via standard nuclear electronics to a two-parameter 4096-channel analyzer operated in a multiplex mode. The over-all resolution was 70 keV FWHM.

#### Proton Beam and Its Detection

In this case a 29.3-MeV proton beam was accelerated and transported to a 130-cm-diam scattering chamber on beam line 6 (see Fig. 1). Because of the great range of 30-MeV protons in silicon, over 5000  $\mu$ , a lithium-drifted germanium detector was used as a particle detector. A planar 10 000- $\mu$  depletion-depth Ge(Li) detector with a 2.54-cm<sup>2</sup>

area was mounted in a vacuum housing with a 0.000 25-mm nickel entrance window. During an experimental run, it was placed in a cryostat located on a movable arm inside the 130-cm-diam scattering chamber. Fill and vent lines for liquid nitrogen were provided to this internal cryostat. The complete detector system has been described elsewhere.<sup>17</sup>

Because of the susceptibility of Ge(Li) detectors to neutron damage, the beam of protons was re-focused after it passed through the target. It was then bent vertically through  $15^\circ$ , and stopped in a well-shielded split Faraday cup (Fig. 3). The split Faraday cup was used to obtain signals for a feedback circuit based on a differential amplifier.<sup>18</sup> This circuit controlled the current in the  $15^\circ$  magnet and insured that the beam would remain centered in the Faraday cup.

Other aspects of the experiment were similar to the  $\alpha$  experiment. The over-all energy resolution in this experiment was approximately 60 keV FWHM. A typical spectrum is shown in Fig. 4.

#### Target Preparation

The  $^{144}\text{Sm}$  targets were prepared from a 95% enriched isotope obtained from the Oak Ridge National Laboratory isotopes sales division. The  $\text{Sm}_2\text{O}_3$  was reduced in a tantalum-tube electron gun by heating in the presence of lanthanum metal to a temperature of approximately  $1500^\circ\text{F}$ . The reaction  $\text{Sm}_2\text{O}_3 + 2\text{La} \rightarrow 2\text{Sm} + \text{La}_2\text{O}_3$  was used to form 0.8- to 2.5-mg/cm<sup>2</sup> metal films on previously prepared glass slides. The slides were prepared by coating them with a thin substrate of NaCl by vacu-

um evaporation. The Sm metal was then floated off in a water bath and picked up on aluminum frames to form self-supporting metal targets. The foils could be handled in air, but prolonged exposure to air did cause oxidation, as can be seen in the peaks caused by oxygen contamination in Figs. 2 and 4. Twenty-four-hour exposure would cause the total oxidation of a 1-mg/cm<sup>2</sup> target.

### III. GENERAL CONSIDERATIONS

#### Optical Model

The elastic scattering data were analyzed in terms of the optical model using the conventional optical-model potential:

$$U(r) = V_C(r) - V_0(e^x + 1)^{-1} - i \left( W_S - 4W_D \frac{d}{dx} \right) (e^{x'} + 1)^{-1} + V_{so} \left( \frac{\hbar}{m_\pi c} \right)^2 \frac{1}{r} \frac{d}{dr} (e^{x_{so}} + 1)^{-1} \vec{l} \cdot \vec{\sigma}, \quad (1)$$

where  $x = (r - R_0)/a_0$ ,  $x' = (r - R')/a'$ ,  $x_{so} = (r - R_{so})/a_{so}$  with  $R_0 = r_0 A^{1/3}$ , etc., and  $V_C(r)$  is the Coulomb potential for a uniformly charged sphere of radius  $R_C = r_C A^{1/3}$ . The optical-model parameter search was carried out using the search code JIB3,<sup>19</sup> which searches for the parameters of the potential which minimize the quantity

$$\chi^2 = \frac{1}{n} \sum_{i=1}^n \left[ \frac{\sigma_{th}(\theta_i) - \sigma_{ex}(\theta_i)}{\Delta \sigma_{ex}(\theta_i)} \right]^2. \quad (2)$$

For  $\alpha$  scattering the imaginary part of the potential was restricted to a volume term only. The

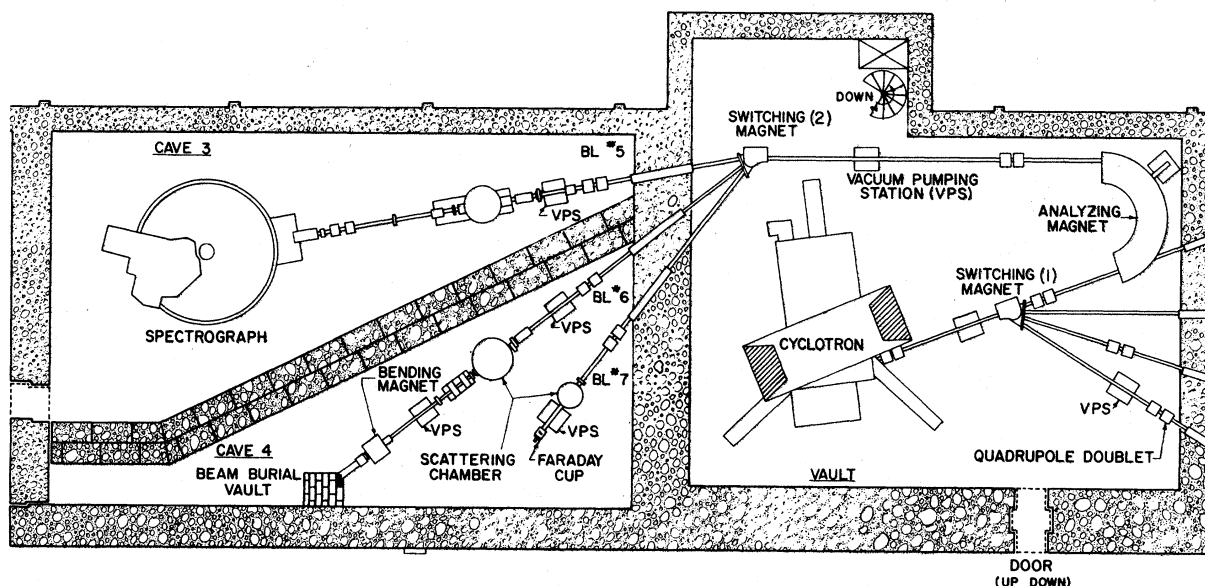


FIG. 1. General experimental setup.

Coulomb radius was taken to be  $r_c = 1.4$  fm. This was not subjected to a search, since the results are insensitive to small changes in its value.<sup>20</sup>

In the analysis of the proton scattering both a surface and a volume imaginary term were included. Extensive searches employing only a surface imaginary term were also performed but equivalent fits could not be obtained.  $\chi^2$  values using only the surface term were approximately twice that obtained when both a surface and volume term were used. More significantly, the  $\chi^2$  values for the inelastic distorted-wave-approximation (DWA) predictions based on the two optical model potentials also exhibited this same relationship. Figures 5 and 6 show the elastic scattering data for the two experiments. The final parameter sets for the optical potentials are given in Table I.

#### Distorted-Wave Approximation

The inelastic scattering angular distributions were analyzed employing the conventional DWA. The transition amplitude is calculated assuming that the projectile excited vibrational states that are described by a collective-model Hamiltonian. The analysis has been restricted to one-step transitions and has been discussed in detail by Bassel *et al.*<sup>20</sup> and Rost.<sup>21</sup> The model treats the inelastic scattering in terms of a nonspherical nuclear potential whose shape oscillates about a spherical

mean. The first term in a Taylor expansion of this potential about the mean radius  $R$  accounts for the one-phonon excitations of a spherical even- $A$  nucleus. All model dependence of the DWA transition amplitude is contained in the reduced matrix element

$$\langle J_f = l \| V_l \| J_i = 0 \rangle = i^l (2l + 1)^{-1/2} F_l(r), \quad (3)$$

where the nuclear form factor is

$$F_l(r) = \beta_l \left[ \frac{VR_0}{a} \frac{d}{dx} f(x) + \frac{iWR'}{a'} \frac{d}{dx'} g(x') \right]. \quad (4)$$

The optical potential

$$U = -Vf(x) - iWg(x), \quad (5)$$

is assumed in deriving this form for Eq. (4). The "deformation parameter"  $\beta_l$  is just the rms deformation in the ground state due to zero-point oscillations. Except for the magnitude of  $\beta_l$ , the nuclear form factor is completely determined by the optical model potential which describes the elastic scattering.

The inelastic cross section for exciting a state with spin  $J = l$  reduces to the form<sup>14</sup>

$$\frac{d\sigma}{d\Omega}(0-l) = \beta_l^2 \sigma_l(\theta), \quad (6)$$

in which the deformation parameter  $\beta_l$  is determined in the comparison of the measured cross

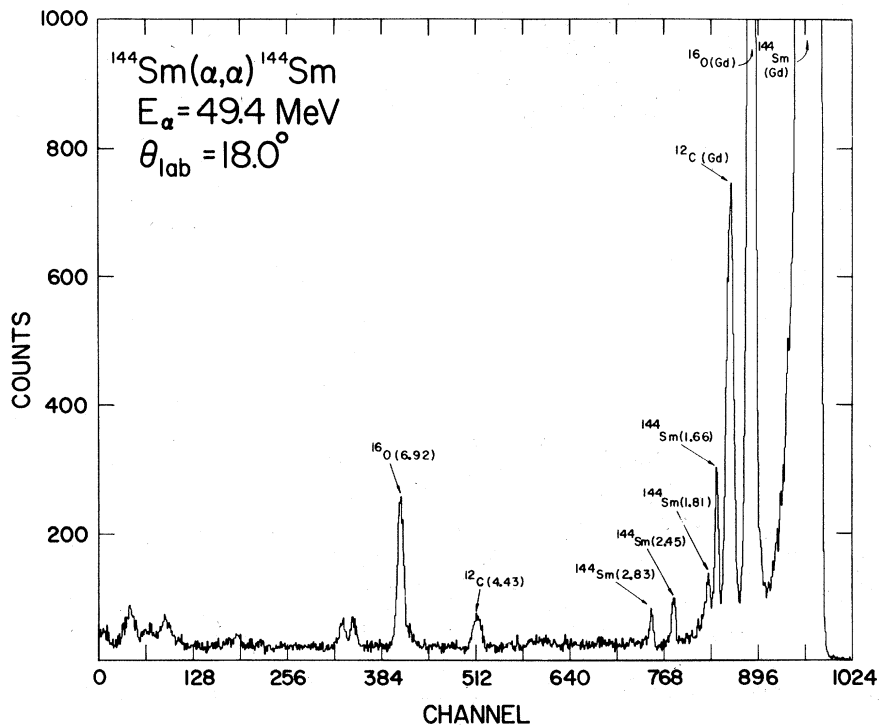


FIG. 2. Experimental spectrum for the  $(\alpha, \alpha')$  experiment.

sections with the DWA prediction  $\sigma_i(\theta)$ .

In order to appreciate the distinction between an electromagnetic (EM) transition rate and a transition rate measured by inelastic scattering it is necessary to compare the form of the different multipole operators responsible for the transitions. The EM multipole operator is given by

$$O(\text{EM}) = \sum_{\text{protons}} r^l Y_l^m(\Omega) = \sum_{\text{nucleons}} \frac{1 + \tau_z}{2} r^l Y_l^m(\Omega). \quad (7)$$

If we restrict ourselves to  $(\alpha, \alpha')$  scattering, then it is possible to define an isoscalar transition operator

$$O(\text{IS}) = \frac{Z}{A} \sum_{\text{nucleons}} r^l Y_l^m(\Omega). \quad (8)$$

One notes immediately that  $O(\text{EM})$  is effective only on protons, while  $O(\text{IS})$  acts on both protons and neutrons. This means that transition strengths derived from  $O(\text{EM})$  are charge-related and those derived from  $O(\text{IS})$  are mass-related. From these definitions, it can be shown<sup>14</sup> that in the vibrational model the reduced EM transition rate and the reduced IS transition rate are numerically equal:

$$B(El) = B(\text{IS}l) = (Z\beta_m C)^2 \left[ \int \rho(r) r^{l+2} dr \right]^2, \quad (9)$$

where  $C$  is the equilibrium radius and  $\beta_m$  is the rms deformation in the mass distribution.

If one assumes a sharp-edge cutoff for the mass distribution, then one obtains from Eq. (9)

$$B(El) = B(\text{IS}l) = (3ZR_\mu^l \beta_m / 4\pi)^2, \quad (10)$$

where  $R_\mu = 1.2A^{1/3}$  is the normal choice for the cutoff radius. If a more correct, rounded-edge distribution is used for  $\rho(r)$ , then Eq. (9) must be

evaluated numerically. Owen and Satchler<sup>22</sup> have evaluated Eq. (9) using a Fermi distribution. The ratio of  $B(El)_{\text{sharp cutoff}}$  to  $B(El)_{\text{Fermi}}$  has been published. This allows one to use the closed-form definition, Eq. (10), and apply a tabulated correction factor.

Equation (10) clearly gives a transition strength that is highly dependent on the size of the system. In order to eliminate this size dependence, transition strengths are often given in single-particle units

$$G(El) = \frac{B(El)}{B_{\text{S.P.}}(El)}, \quad (11)$$

where

$$B_{\text{S.P.}}(El) = \frac{(2l+1)}{4\pi} \left( \frac{3}{3+l} \right)^2 (R_\mu)^{2l}. \quad (12)$$

This leads to

$$G(El) = G(\text{IS}) = \frac{(Z\beta_m)^2 (3+l)^2}{4\pi(2l+1)}. \quad (13)$$

Equation (6) indicates that if the collective model is used then the DWA formalism completely predicts the shape of inelastic angular distributions. Only one parameter is free to be adjusted, and that is the deformation parameter  $\beta_l$ . It is incorrect at this point to identify  $\beta_l$  and  $\beta_m$  with each other.

It was remarked earlier that the nuclear radius parameters  $R_0$  and  $R'$  are influenced by the type of projectile. Equation (4) indicates that  $R_0$  and  $R'$  must in fact enter the calculation of the cross section as a cofactor of  $\beta_l$ . Thus  $\beta_l$  will also be dependent on the choice of projectile.

It has been pointed out<sup>14,23</sup> that the more proper

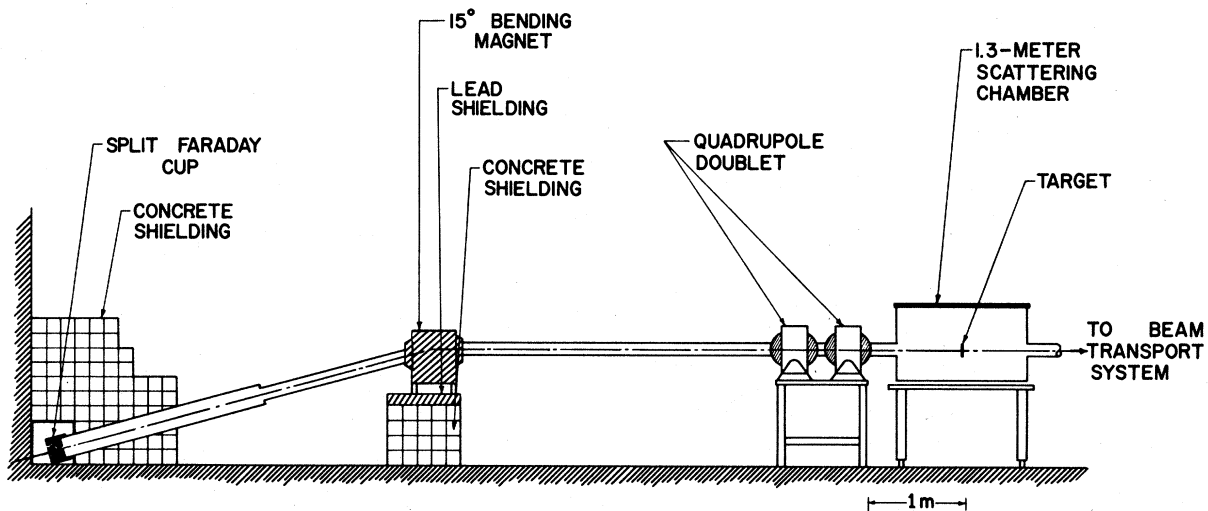


FIG. 3. Side-view detail of beam line No. 6 showing split Faraday cup and 15° bending magnet.

parameters to compare are  $\beta_l R'$  and  $\beta_m R_\mu$ . The basic premise is that the magnitude of the mass-vibration and the optical-potential deformation length should be equal. When different geometries are used in the real and imaginary parts of the potential the comparison is made more difficult. The suggestion of Bernstein<sup>14</sup> that  $R'$  is the proper parameter to use will be employed in this analysis. It leads to the following key equation:

$$\beta_l R' = \beta_m R_\mu. \quad (14)$$

In order to calculate a transition strength, one first employs Eq. (14) to obtain an "equivalent mass value" for  $\beta_m$ . This value is then substituted into Eq. (13). The transition rate obtained must then be corrected via the tables of Owen and Satchler<sup>22</sup> or Bernstein<sup>14</sup> for the error introduced by using a sharp-cutoff model.

#### IV. EXPERIMENTAL RESULTS

It is well established that the shapes of the angular distributions predicted by the DWA offer a good means for determining both the  $l$  transfer and parity of excited levels. If the ground state has  $J^\pi = 0^+$ , then the spin of the excited state is also determined. In the case of  $\alpha$  scattering, the parity is easily determined by the Blair phase rule. The  $l$  transfer can be ascertained from a comparison

TABLE I. Optical-potential parameters.

$U(r)$	$(\alpha, \alpha')$	$(\rho, \rho')$
$V_0$	185.0 MeV	53.7 MeV
$r_0$	1.40 fm	1.17 fm
$a_0$	0.52 fm	0.71 fm
$W_S$	25.8 MeV	2.13 MeV
$W_D$	...	7.5 MeV
$r'$	1.33 fm	1.27 fm
$a'$	0.49 fm	0.65 fm
$V_{so}$	...	5.97 MeV
$r_{so}$	...	1.09 fm
$a_{so}$	...	0.71 fm
$r_C$	1.4 fm	1.2 fm

of the shapes of the experimental and predicted angular distributions.

The major difficulty in the  $\alpha$  experiment is the need for small-angle data in order to make spin assignments. A comparison of the angular distributions (Figs. 6 and 7) reveals that for angles greater than  $30^\circ$  the data are in excellent agreement with the Blair phase rule. That is, the one observed odd-parity state at 1.81 MeV is in phase with the elastic scattering and the three even-parity states are in phase with each other and out of phase with the elastic scattering. Because of the similarity of shapes at angles greater than  $30^\circ$ , it is impossible to distinguish between  $2^+$  and  $4^+$  an-

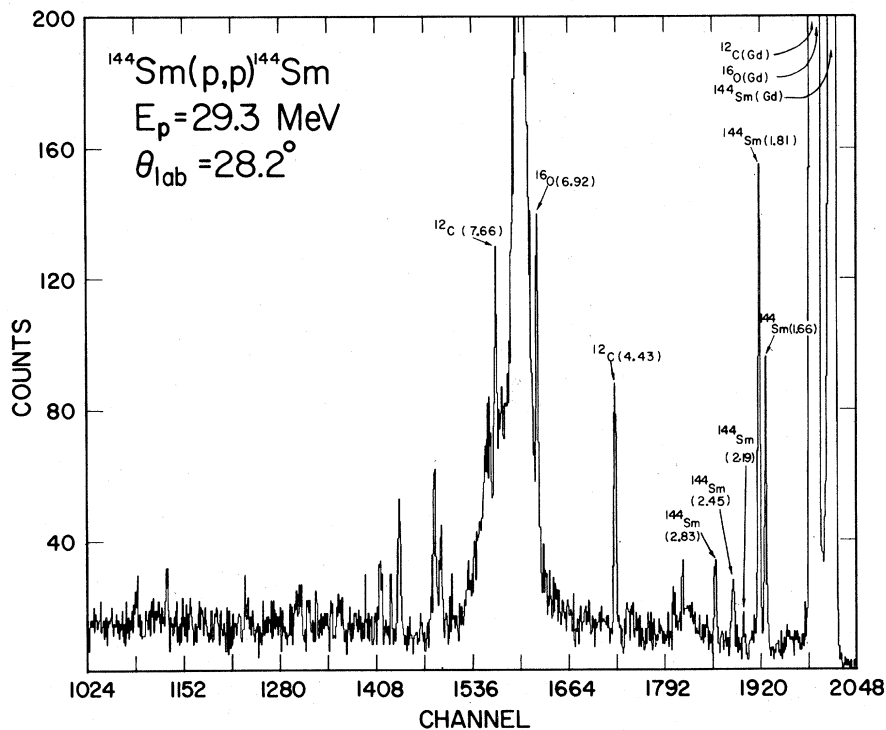


FIG. 4. Experimental spectrum for the  $(p, p')$  experiment.

gular distributions in this region. The angular momentum signature is only evident at angles less than  $20^\circ$ .

It is also clear (Fig. 7) that if one hopes to analyze the forward-angle scattering data to determine the  $l$  transfer, Coulomb-excitation effects must be included. Including Coulomb excitation to  $\theta \sim 10^\circ$  requires the use of approximately 100 partial waves in the DWA calculation.<sup>20</sup> The actual calculations were carried out with the DWA code DWUCK.<sup>24</sup> The use of 50 partial waves (not shown) led to a markedly worse fit. Reference 6 gives a more detailed example of this effect.

The level at 1.66 MeV is well established as a  $2^+$  state,<sup>8</sup> and good agreement is obtained between experiment and DWA predictions assuming a  $l=2$  transfer. The  $3^-$  level at 1.81 MeV is also well established,<sup>9</sup> and again good agreement is obtained between experiment and a DWA prediction for a  $l=3$  transfer. The level at 2.21 MeV has recently been given a  $4^+$  designation on the basis of  $\gamma$ -ray systematics<sup>7</sup> and our data verify this assignment. We assign  $J^\pi=2^+$  to the state excited at  $2.45 \pm 0.02$  MeV on the basis of the similarity of its angular distribution to that of the well established  $2^+$  level at 1.66 MeV. A group at 2.83 MeV (Fig. 2) appeared to be an unresolved multiplet. No attempt was made to extract its members, although

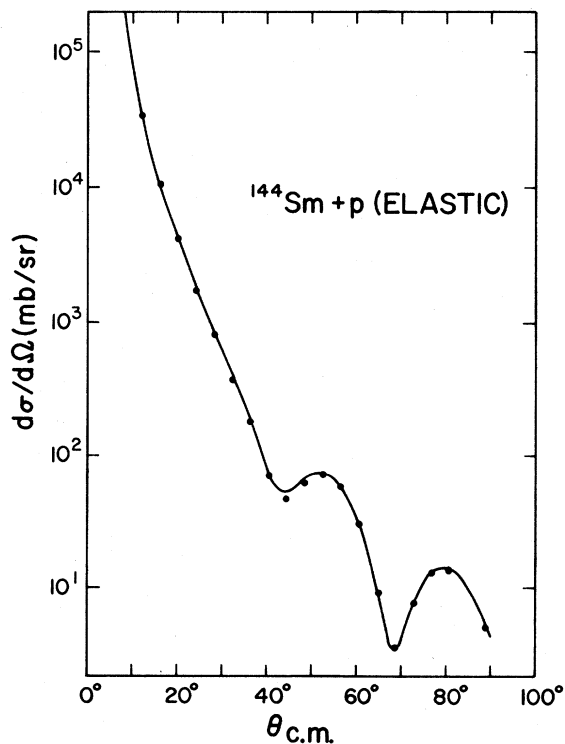


FIG. 5.  $^{144}\text{Sm}(p,p)$  elastic scattering angular distribution.

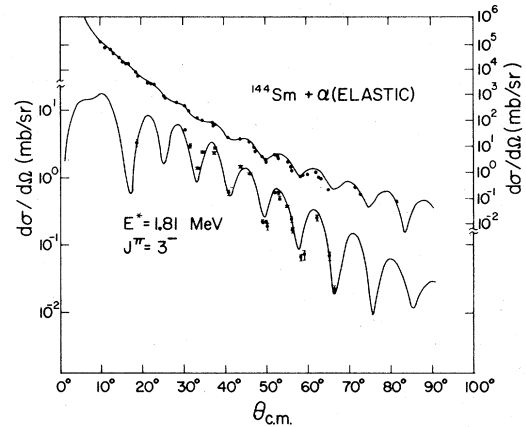


FIG. 6. Comparison of the measured elastic  $\alpha$ -particle angular distribution with the optical model fit (right scale) and the inelastic angular distribution for the  $3^-$  state at 1.81 MeV in  $^{144}\text{Sm}$  with the DWA prediction (left scale). The oscillations in the differential cross sections are in phase as is expected.

a featureless angular distribution indicates that either opposite-parity states are excited or multiple-excitation processes are contributing.

In the case of the proton angular distributions (Fig. 8) there is no longer a need to obtain small-

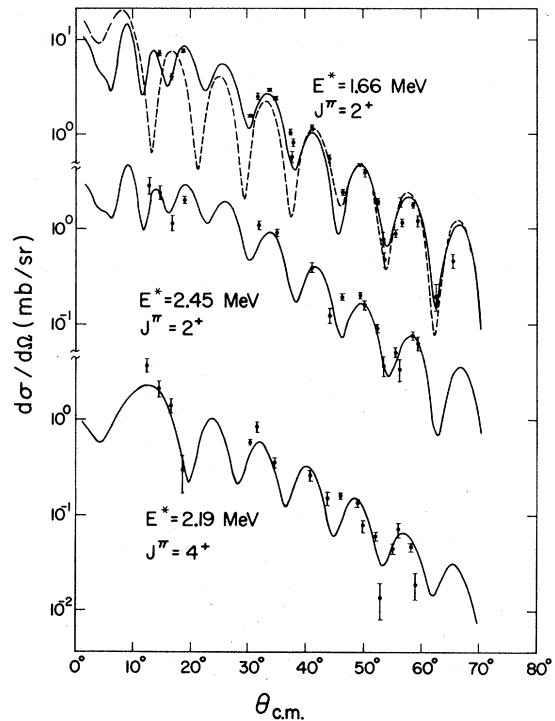


FIG. 7. Inelastic angular distribution measured for  $^{144}\text{Sm}(\alpha, \alpha')$  reactions. The solid curves are DWA predictions including Coulomb excitation. The dashed curve corresponds to the identical nuclear scattering prediction with no Coulomb excitation included.

angle data, since the angular distributions carry their angular momentum signature at larger angles. The Blair phase rule cannot be applied, but the shapes of the DWA predicted angular distributions are sufficiently different so as to allow the unambiguous assignment of both spin and parity to the strongly excited levels we observed. All levels observed in the  $\alpha$ -particle work were also observed in the proton work, and no new levels were observed.

The spin and parity assignments from the proton study are identical to those of the  $(\alpha, \alpha')$  analysis. The assignment of a  $2^+$  designation to the level at 2.45 MeV is again verified on the basis of the similarity of its proton angular distribution to that of the well-established  $2^+$  level at 1.66 MeV. In

these reactions Coulomb excitation has a smaller effect on the small-angle shape of the DWA prediction. The states at 1.81 and 2.19 MeV have proton angular distributions in excellent agreement with DWA predictions for a  $3^-$  and  $4^+$  level, respectively.

V. DISCUSSION

Spin and Parity Assignments

A comparison of our level scheme for  $E^* \leq 2.83$  MeV, Fig. 9, with the other experimental determinations leads to apparent discrepancy in the spin assignment of the level at 2.45 MeV. A level near this energy has already been the subject of some controversy.<sup>10,11</sup> From our data it would appear that there are two levels near this energy. A level with  $J^\pi = 0^+$  and  $E^* = 2.481$  MeV has been reported<sup>7,11,12</sup> as being populated by the  $\beta$  decay of  $^{144}\text{Eu}$ . We report a second level with  $J^\pi = 2^+$  and  $E^* = 2.45 \pm 0.02$  MeV that is directly excited by  $(d, d')$ ,<sup>10</sup>  $(\alpha, \alpha')$ , or  $(p, p')$  reactions. Previous descrip-

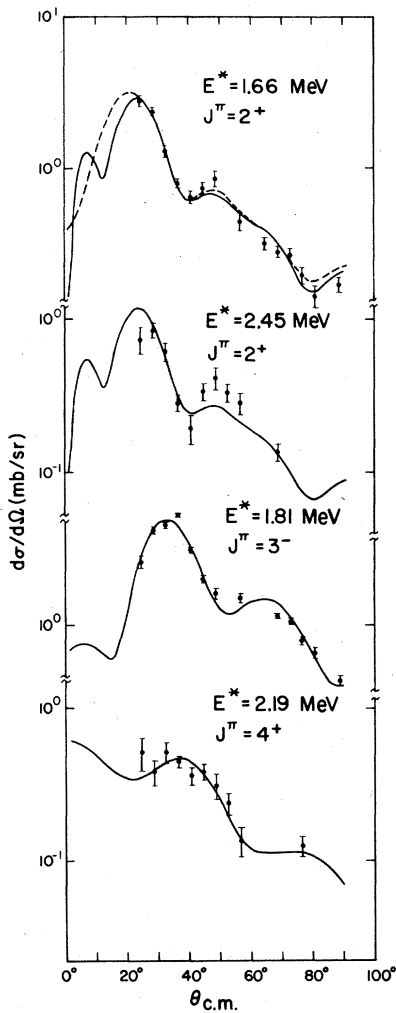
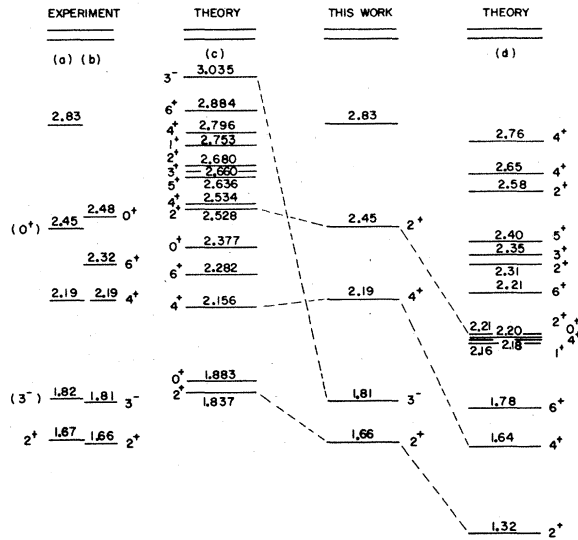


FIG. 8. Inelastic angular distribution measured for  $^{144}\text{Sm}(p, p')$  reactions. The solid curves are DWA predictions including Coulomb excitation. The dashed curve corresponds to the identical nuclear scattering prediction with no Coulomb excitation included.



0.0  $0^+$     0.0  $0^+$     0.0  $0^+$     0.0  $0^+$

FIG. 9.  $^{144}\text{Sm}$  energy-level diagram: (a) Ref. 9, (b) Ref. 12, (c) Ref. 3, (d) Ref. 25.

tions of this level have assumed it was the  $0^+$  level seen in the  $\beta$ -decay experiments.

A comparison of the experimental data with the theoretical work of Wildenthal shows good qualitative agreement. The dashed lines (Fig. 8) can most probably be trusted for the first  $2^+$  and  $4^+$  levels but should be regarded as suggestive for the second  $2^+$ . His theoretical model allows protons to occupy only the  $1g_{7/2}$  and  $2d_{5/2}$  levels and so neglects several significant configurations. This has two effects: First, it does not allow the computation of negative-parity states; and second, it is probably responsible for an over-all energy shift for the computed levels.<sup>25</sup>

A comparison with the theoretical work of Waroquier and Hyde<sup>3</sup> also shows good agreement for the low-lying levels. A notable exception is their prediction for the first  $3^-$  level. The authors point out that their calculations systematically overestimate the energy of the first  $3^-$  state, and that by working in a larger model space they hope to correct this.

#### Transition Strengths

As can be seen from Eq. (6), the DWA predictions for the angular distributions completely determine their shape; only the normalization parameter  $\beta_1^2$  is left undetermined.  $\beta_1^2$  is extracted by doing a least-squares fit of the predicted angular distributions to the experimental distributions. Figures 6 and 7 are the result of such a fitting procedure. The  $\beta_1 R'$  obtained in this manner are presented in Table II.

It has been pointed out<sup>14</sup> that  $\beta_1 R'$  values extracted with  $(\alpha, \alpha')$  reactions should be more reliable than those obtained from the inelastic scattering of other more penetrating particles. Since  $(\alpha, \alpha')$  scattering is a surface reaction, the DWA predictions should be relatively free of the ambiguities of the optical potential used to obtain the distorted waves. All such potentials yield wave functions that agree in the surface region but tend to differ in the nuclear interior.

For protons the interior contributions may be of more significance. Our data (see Table II) as well

as that of others<sup>14,26</sup> seem to indicate that these interior contributions are relatively minor for strongly excited vibrational states. Our  $\beta_1 R'$  values extracted from the two experiments are found to agree quite well. The absolute error in their magnitude is estimated to be  $\pm 15\%$ . The observed equality of the strengths implies that the spin-flip and isospin-flip amplitudes are negligible for the  $(p, p')$  reactions. The difference between the EM and IS measurements of the strength for the first  $2^+$  state exceeds our quoted uncertainty. At present, it is not possible to comment as to whether this difference contains significant information on the structure of  $^{144}\text{Sm}$ . No systematic differences can be seen in previous comparisons,<sup>14</sup> indicating that more-precise measurements on many nuclei are required.

It is of interest to compare the available data on deformation lengths for the  $N=82$  nuclei. Inelastic  $\alpha$ -particle scattering data for  $^{140}\text{Ce}$  have been reported<sup>27</sup> and similar data for  $^{138}\text{Ba}$  are available.<sup>28</sup> Measured deformation lengths for the first excited  $2^+$  states are 0.43 fm for  $^{144}\text{Sm}$ , 0.49 fm for  $^{140}\text{Ce}$ , and 0.42 fm for  $^{138}\text{Ba}$ . Corresponding values of  $\beta_3 R'$  for the lowest  $3^-$  states are 0.71 fm for  $^{144}\text{Sm}$ , 0.66 fm for  $^{140}\text{Ce}$ , and 0.59 fm for  $^{138}\text{Ba}$ . The relative similarity of the  $\beta_2 R'$  values compared to the increasing trend of  $\beta_3 R'$  values with atomic number suggests that the  $2^+$  states are predominantly core vibrations, whereas the  $3^-$  states include the extracore protons in a significant way.

Since EM and IS rates are formally equal only for nuclei where  $N=Z$ , it is not totally correct to compare theoretical EM rates with the IS rates measured in these experiments. Such a procedure will only be valid in so far as the vibrational collective model is a good description of these nuclei. Bernstein has published tables of comparisons of EM and IS rates that indicate an average agreement of 30%. It is in the spirit of this observed empirical agreement that comparisons are made in the remainder of this section.

The comparison of experimental and theoretical transition rates in Table II shows reasonable qualitative agreement. The theoretical value for the

TABLE II. Transition strengths.

$J^\pi$	$E^*$ (MeV)	$(\alpha, \alpha')$		Experiment		$(^{16}\text{O}, ^{16}\text{O})$ (Ref. 13) $G(EI)$	Theory (Ref. 3)	
		$\beta_1 R'$ (fm)	$G(l)$	$\beta_1 R'$ (fm)	$G(l)$		Surface $\delta$ interaction $G(EI)$	Gaussian interaction $G(EI)$
$2^+$	1.66	0.43	7.0	0.44	6.6	11.0	7.6	11.0
$3^-$	1.81	0.71	20.8	0.82	24.4	...	...	10.0
$4^+$	2.19	0.30	4.2	0.32	4.3	...	...	...
$2^+$	2.45	0.26	2.5	0.29	2.9	...	...	1.6

first  $2^+$  level happens to be in good agreement with our experimental numbers when a surface- $\delta$  interaction is used. The predicted transition rate increases when the more realistic Gaussian interaction is employed, bringing it into good agreement with the Coulomb-excitation measurement. Qualitative agreement is obtained between experiment and theory for the second  $2^+$  state. The collective  $3^-$  octupole state shows a strong enhancement, with the theory underestimating the magnitude of the enhancement. Waroquier and Hyde<sup>3</sup> note that their two-quasiparticle space is inadequate for the description of the  $3^-$  state, resulting in the reduced theoretical enhancement.

#### VI. CONCLUSION

The scattering of 50-MeV  $\alpha$  particles and 30-MeV protons by  $^{144}\text{Sm}$  has been analyzed in terms of the vibrational model. As expected, the deeper penetration of the protons does not lead to significantly different results when the states involved are the strongly excited collective states. The measured strengths agree to within  $\pm 15\%$  in all cases. Complex potentials with different real and imaginary geometries were used in the analysis, and the imaginary radii were used in the quoted  $\beta_1 R'$  values.

Recent shell-model calculations<sup>3,25</sup> are in reasonably good agreement with the available experimental data. The relative locations of the strongly excited positive-parity states are accurately predicted. The predicted location of the first  $3^-$

state is not accurate owing to the restricted model space, composed of the  $n=4$  oscillator shell and the  $1\hbar_{11/2}$  proton orbit.<sup>3</sup> The theoretical electromagnetic transition rates<sup>3</sup> show qualitative agreement with the measured isoscalar rates. Our understanding of the detailed differences between EM and IS transition rates is not yet sufficient to permit any discussion of these differences. A comparison with the inelastic  $\alpha$  scattering from other even-even  $N=82$  nuclei suggests that the first  $2^+$  states are not strongly affected by the number of extracore protons, whereas the  $3^-$  transition rates appear to vary smoothly with  $Z$ .

Based on both the  $(\alpha, \alpha')$  and  $(p, p')$  experiments we have assigned  $J^\pi = 2^+$  to a level at  $2.45 \pm 0.02$  MeV. The  $4^+$  assignment for the level at 2.190 MeV is confirmed by both inelastic reactions exciting this state. No conclusions are made concerning the level(s) at 2.83 MeV in  $^{144}\text{Sm}$  due to the lack of structure in the angular distributions.

#### ACKNOWLEDGMENTS

We wish to thank the Cyclotron Institute staff for their assistance throughout this project. In particular we acknowledge the help of W. Lozowski and J. Lovelady in the preparation of the  $^{144}\text{Sm}$  targets. We are grateful to P. D. Kunz for supplying the distorted-wave code DWUCK and for helpful discussions concerning its application to this problem. We also thank B. H. Wildenthal for communicating some results of his shell-model calculations prior to publication.

†Work supported in part by the Robert A. Welch Foundation and the U. S. Atomic Energy Commission.

\*Present address: Washington University, St. Louis, Missouri.

<sup>1</sup>B. H. Wildenthal, *Phys. Rev. Letters* **22**, 1118 (1969).

<sup>2</sup>M. Waroquier and K. Hyde, *Nucl. Phys.* **A144**, 481 (1970).

<sup>3</sup>M. Waroquier and K. Hyde, *Nucl. Phys.* **A164**, 113 (1971).

<sup>4</sup>E. Newman, K. S. Toth, R. L. Augle, R. M. Gaedke, M. F. Roche, and B. H. Wildenthal, *Phys. Rev.* **1**, 1118 (1970).

<sup>5</sup>B. H. Wildenthal, E. Newman, and R. L. Auble, *Phys. Rev. C* **3**, 1199 (1971).

<sup>6</sup>F. T. Baker and R. Tickle, *Phys. Letters* **32B**, 47 (1970).

<sup>7</sup>J. Kowacki, Z. Sujkowski, L. E. Fraberg, H. Ryde, and I. Adam, in *Proceedings of the International Conference on Nuclear Structure, Montreal, 1969*, edited by M. Harvey *et al.* (Presses de l'Université de Montréal, Montreal, Canada, 1969).

<sup>8</sup>O. Hanson and O. Nathan, *Nucl. Phys.* **42**, 197 (1963).

<sup>9</sup>*Nucl. Data* **B2**, 74 (1967).

<sup>10</sup>P. R. Christensen and F. C. Yang, *Nucl. Phys.* **72**, 657 (1965).

<sup>11</sup>J. S. Geiger and R. L. Graham, *Arkiv Fysik* **36**, 191 (1966).

<sup>12</sup>J. Kownacki, I. Jarosiewicz, V. Serejev, Z. Sujkowski, and H. Ryde, Research Institute for Physics Annual Report, Stockholm, 1970 (unpublished).

<sup>13</sup>D. Eccleshall, M. J. L. Yates, and J. J. Simpson, *Nucl. Phys.* **78**, 481 (1966).

<sup>14</sup>A. M. Bernstein, in *Advances in Nuclear Physics*, edited by M. Baranger and E. Vogt (Plenum, New York, 1969), Vol. III, p. 335.

<sup>15</sup>B. M. Bardin and M. E. Rickey, *Rev. Sci. Instr.* **35**, 902 (1964).

<sup>16</sup>R. A. Kenefick, J. C. Hiebert, and C. W. Lewis, *Nucl. Instr. Methods* **88**, 13 (1970).

<sup>17</sup>F. E. Bertrand, R. W. Peele, T. A. Love, N. W. Hill, and W. R. Burrus, Oak Ridge National Laboratory Report No. ORNL-4274, 1968 (unpublished).

<sup>18</sup>R. C. Rogers and R. A. Kenefick, *Nucl. Instr. Methods* **86**, 313 (1970).

<sup>19</sup>F. G. Perey, unpublished.

<sup>20</sup>R. H. Bassel, G. R. Satchler, R. M. Drisko, and

E. Rost, Phys. Rev. **128**, 2693 (1962).

<sup>21</sup>E. Rost, Phys. Rev. **128**, 2708 (1962).

<sup>22</sup>L. W. Owen and G. R. Satchler, Nucl. Phys. **51**, 155 (1964).

<sup>23</sup>J. S. Blair, in *Proceedings of the International Conference on Nuclear Structure, Kingston, 1960*, edited by D. A. Bromley and E. W. Vogt (University of Toronto Press, Toronto, 1960).

<sup>24</sup>P. D. Kunz, unpublished.

<sup>25</sup>B. H. Wildenthal, private communication.

<sup>26</sup>J. C. Bane, J. J. Kraushaar, B. W. Ridley, and M. M. Stautber, Nucl. Phys. **A116**, 580 (1968).

<sup>27</sup>F. T. Baker and C. Ellegaard, to be published [quoted by H. W. Baer *et al.*, Phys. Rev. C **3**, 1398 (1971)].

<sup>28</sup>J. H. Barker and J. C. Hiebert, to be published.

PHYSICAL REVIEW C

VOLUME 4, NUMBER 6

DECEMBER 1971

## Study of the Energy Levels of $^{112}\text{Cd}$ Using Nuclear Photoexcitation

R. Moreh and A. Nof

*Nuclear Research Center, Negev, Beer Sheva, Israel*

(Received 18 June 1971)

Elastic and inelastic scattering of monochromatic photons were used for studying nuclear energy levels in  $^{112}\text{Cd}$ ; the photons were produced by thermal-neutron capture in iron. The energy of the resonance level was 7632 keV; it was found to decay to 19 known low-lying energy levels in  $^{112}\text{Cd}$ . The angular distributions of the elastic and inelastic lines were measured and the following spin-parity determinations were made (energy in keV,  $J^\pi$ ): 617,  $2^+$ ; 1223,  $0^+$ ; 1429,  $0^+$ ; 1468,  $2^+$ ; 1869,  $0^+$ ; 2832,  $0^+$ ; 2850,  $2^+$ ; 3110,  $2^-$ ; 3193,  $2^-$ ; 3247,  $0^-$ ; and 7632,  $1^-$ . The parity of the last level was directly determined by polarization measurements, while the parities of the other levels were inferred from the radiation strength of the corresponding high-energy transitions. The  $M2/E1$  mixing ratio for one primary transition was found to be about 3 orders of magnitude higher than that predicted by the simple theory. The results of statistical analysis of the data are given.

### I. INTRODUCTION

The use of nuclear photoexcitation for studying the energy levels of excited nuclear levels is by now a well-known technique.<sup>1-6</sup> In an earlier publication<sup>1</sup> the potentialities of using the  $(\gamma, \gamma')$  reaction in nuclear studies were discussed in some detail. In this paper, the deexcitation of the 7632-keV levels in  $^{112}\text{Cd}$  photoexcited by the incident  $\gamma$  beam from  $\text{Fe}(n, \gamma)$  has been studied using a Ge(Li) detector.

The energy levels of  $^{112}\text{Cd}$  were studied earlier by several methods using the  $^{111}\text{Cd}(d, p)$  reaction,<sup>7</sup> the  $^{112}\text{Cd}(p, p')$  reaction,<sup>8</sup> and the  $\beta$  decay of  $^{112}\text{Ag}$ .<sup>9</sup> The levels of  $^{112}\text{Cd}$  were also studied by several investigators using a  $(\gamma, \gamma')$  reaction<sup>2, 3, 10, 11</sup>; in particular, the angular distribution of the scattered radiation spectrum was measured, thus providing information on the spins of four levels and the quadrupole-dipole mixing ratio for one high-energy transition. In the present work more information regarding the energies and spins of the low-lying levels in  $^{112}\text{Cd}$  was obtained. The  $M2/E1$  mixing ratios for the high-energy transitions were deduced. In addition, some statistical analysis of the partial radiative widths of the 7632-keV level is presented. A short report of the present work was published elsewhere.<sup>12</sup>

### II. EXPERIMENTAL METHOD

Thermal neutrons were provided by the Israel Research Reactor-2 (IRR-2). The  $\gamma$ -ray source was produced by neutron capture in five separated disks of iron placed along a tangential beam port near the reactor core; details of the experimental system were published previously.<sup>1</sup> The  $\gamma$  beam was collimated, neutron-filtered, and allowed to hit a metallic Cd scatterer. The scattered  $\gamma$  radiation was measured by using Ge(Li) and NaI(Tl) detectors. The energy resolution of the Ge(Li) detector was about 18 keV for the 7632-keV line. Time normalization in angular-distribution measurements was achieved by monitoring the  $\gamma$  beam using a NaI detector. The energy calibration and the variable-energy response of the Ge(Li) detectors were measured using the well-known  $\gamma$ -line energies and intensities<sup>13</sup> of the direct  $\text{Fe}(n, \gamma)$  beam.

### III. RESULTS

#### A. Energy Spectrum

High- and low-energy scattered spectra were measured with 30- and 40-cm<sup>3</sup> Ge(Li) detectors. Figure 1 shows the high-energy part of the scattered spectrum using 14-g/cm<sup>2</sup>-thick natural Cd